

Self-regulated non-reciprocal motions in single-material microstructures

<https://doi.org/10.1038/s41586-022-04561-z>

Received: 22 October 2020

Accepted: 17 February 2022

Published online: 4 May 2022

 Check for updates

Shucong Li^{1,5}, Michael M. Lerch^{2,3,5}, James T. Waters⁴, Bolei Deng², Reese S. Martens², Yuxing Yao¹, Do Yoon Kim², Katia Bertoldi², Alison Grinthal², Anna C. Balazs⁴ & Joanna Aizenberg^{1,2,✉}

Living cilia stir, sweep and steer via swirling strokes of complex bending and twisting, paired with distinct reverse arcs^{1,2}. Efforts to mimic such dynamics synthetically rely on multimaterial designs but face limits to programming arbitrary motions or diverse behaviours in one structure^{3–8}. Here we show how diverse, complex, non-reciprocal, stroke-like trajectories emerge in a single-material system through self-regulation. When a micropost composed of photoresponsive liquid crystal elastomer with mesogens aligned oblique to the structure axis is exposed to a static light source, dynamic dances evolve as light initiates a travelling order-to-disorder transition front, transiently turning the structure into a complex evolving bimorph that twists and bends via multilevel opto-chemo-mechanical feedback. As captured by our theoretical model, the travelling front continuously reorients the molecular, geometric and illumination axes relative to each other, yielding pathways composed from series of twisting, bending, photophobic and phototropic motions. Guided by the model, here we choreograph a wide range of trajectories by tailoring parameters, including illumination angle, light intensity, molecular anisotropy, microstructure geometry, temperature and irradiation intervals and duration. We further show how this opto-chemo-mechanical self-regulation serves as a foundation for creating self-organizing deformation patterns in closely spaced microstructure arrays via light-mediated interpost communication, as well as complex motions of jointed microstructures, with broad implications for autonomous multimodal actuators in areas such as soft robotics^{7,9,10}, biomedical devices^{11,12} and energy transduction materials¹³, and for fundamental understanding of self-regulated systems^{14,15}.

Self-regulation is fundamental to complex motion in living systems, but how to design for and harness such emergent behaviour in microscale synthetic materials is not yet well understood. In biology, self-regulated responses emerge from multiple levels of integrated feedback, both within the system and in turn within the stimulus field, intricately orchestrating dynamic movement trajectories with spatial and temporal complexity that are rarely seen in synthetic actuators. For most complex microscale motions demonstrated so far, each position along a trajectory must be either explicitly programmed into the material through fabrication^{4,7,16–19} or directly manipulated in real time by sequential change of external stimuli^{3,5,17,20,21}. Feedback incorporated into materials, for example by multilayer, hierarchical or multi-stimuli-responsive compositions^{22–24}, or embedded chemical reactions and patterning^{25,26}, has led to unique actuation modes or temporal dynamics, but the achieved motions are still largely defined by the underlying architecture or oscillatory dynamics^{27–29}, resulting in a limited set of highly specific, generally two-state movements, with little dynamic pathway control. Harnessing feedback with a stimulus, such

as light or a magnetic field, enables dynamic amplification of phototropic^{25–30} or other behaviours, but without internal feedback it remains difficult to programme complex or diverse motion trajectories into microscale artificial systems. To take self-regulated motion to the next level, both internal and external feedback from a full three-dimensional (3D) space must be integrated, but current trends in addressing this challenge by engineering ever more complexity into hierarchical multimaterial constructs may—in addition to being technically complicated— inadvertantly narrow opportunities for the spontaneous, bottom-up self-integration seen in living systems.

Here we introduce an orthogonal approach to this trend and design simple, compositionally uniform microstructures capable of a vast set of self-regulated motions. We focus on molecularly anisotropic materials that: (1) are aligned non-collinearly to the principal axis of the microstructure; and (2) undergo a stimulus-induced order-to-disorder transition. We hypothesized that these two basic design requirements must be met to invoke and interweave multiple levels of feedback. For example, consider a photosensitive micropost illuminated by a

¹Department of Chemistry and Chemical Biology, Harvard University, Cambridge, MA, USA. ²John A. Paulson School of Engineering and Applied Sciences, Harvard University, Cambridge, MA, USA. ³Stratingh Institute for Chemistry, University of Groningen, Groningen, the Netherlands. ⁴Chemical Engineering Department, University of Pittsburgh, Pittsburgh, PA, USA. ⁵These authors contributed equally: Shucong Li, Michael M. Lerch. ✉e-mail: jaiz@seas.harvard.edu

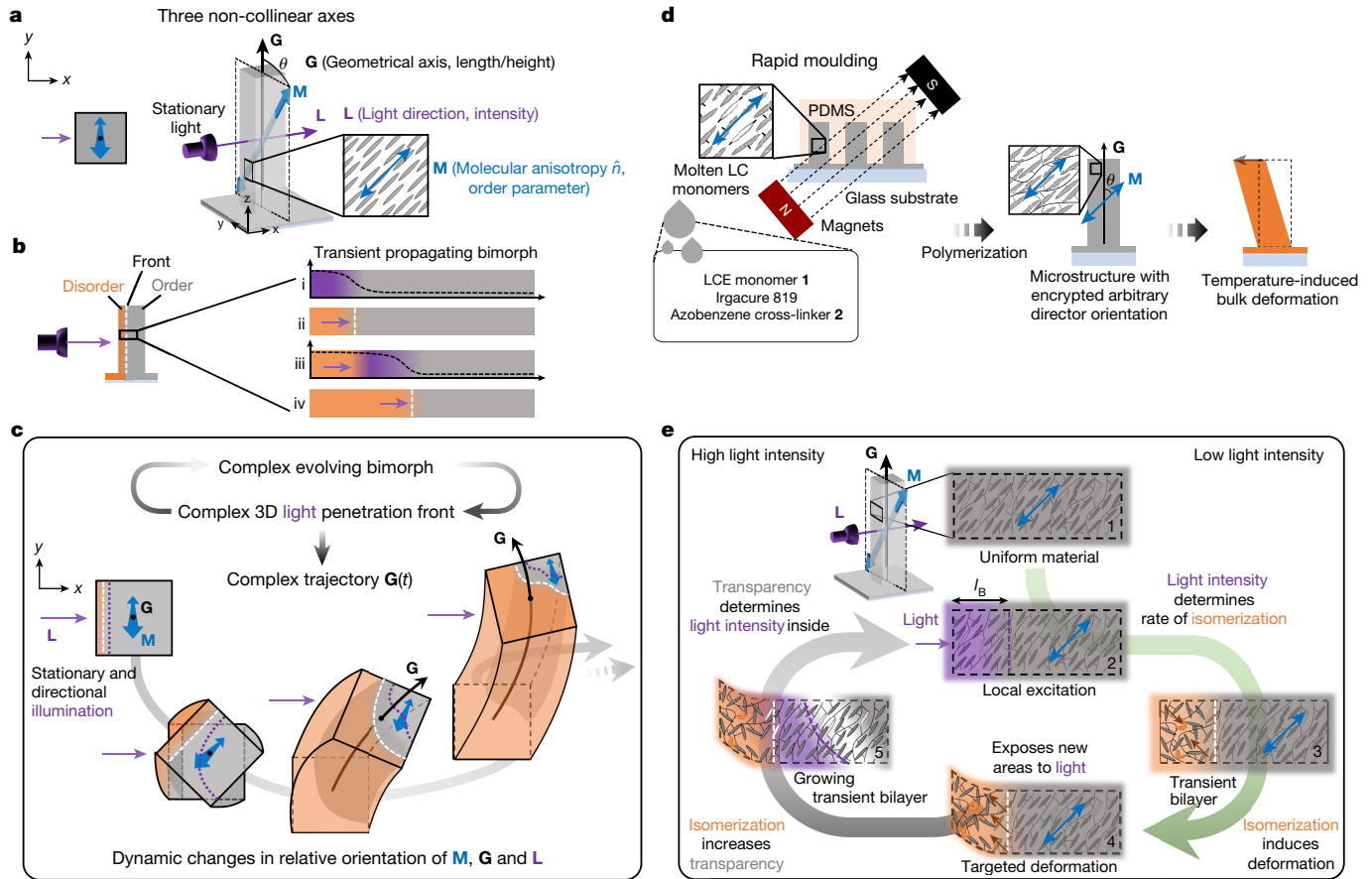


Fig. 1 | Three non-collinear symmetry axes and their dynamic opto-chemo-mechanical feedback enable an infinite set of self-regulated motions in a compositionally uniform microstructure. **a**, Misalignment of molecular anisotropy (**M**), microstructure geometry (**G**) and light (**L**)—each with programmable directionality and magnitude—lays the basis for spatiotemporally diverse microstructure deformation trajectories. **b**, A transient bimorph is formed in a single material by directional light activation (orange represents ‘activated’ and disordered; grey, ‘non-activated’ and ordered) with a stationary light source. The order-to-disorder front (indicated by a white dashed line) self-propagates via induced transparency and leads to a dynamically evolving bimorph: directional illumination (i) locally triggers order-to-disorder transition (ii), which increases the material’s transparency and enables light to penetrate deeper into the structure (iii), resulting in a travelling disorder-to-order front (iv). **c**, Complex deformation trajectory, represented by the changing orientation of **G**(*t*), is produced by feedback between bimorph evolution, complex 3D light penetration profile and the corresponding dynamic

reorientations among the **MGL** axes. **d**, High-aspect ratio microposts are moulded from a photoresponsive liquid crystalline elastomer (LCE; LCE monomer **1**: 4”-acryloyloxybutyl 2,5-di(4’-butyloxybenzoyloxy)benzoate; cross-linker **2**: 4,4'-bis(9-acryloyloxyonyloxy) azobenzene; photoinitiator Irgacure 819: bis(2,4,6-trimethylbenzoyl)-phenylphosphineoxide), and molecular anisotropy is pre-oriented along an arbitrary direction by a magnetic field before polymerization. A photoswitchable azobenzene cross-linker confers light-sensitive disruption of molecular order. Curing of the elastomer locks in the magnetically programmed molecular anisotropy within the microstructure. The liquid crystal (LC) director orientation (denoted by the blue double arrow) determines the bulk deformation. **e**, An opto-chemo-mechanical feedback loop modulates the transiently activated region and is key to complex micropost motion. Both the change in transparency and the material deformations change the light intensity inside the material over time, which then induces further isomerization and deformation.

stationary light source, such that the system’s three primary symmetry elements (molecular anisotropy, **M**, geometrical axis, **G**, and illumination direction, **L**) are all linearly independent in 3D (Fig. 1a). As light enters and triggers a chemically driven order-to-disorder transition in a thin layer of the material, the structure will transiently become a bimorph, in which an initially thin ‘activated’ disordered region (shown in orange) is assumed to self-propagate by induced transparency^{30,31} (Fig. 1b). At the molecular scale, the order-to-disorder transition will generate a directional force normal to—and determined solely by—the initial molecular alignment direction. The subsequent structural deformation will be determined by a combination of this directional force and the orientation of the bimorph interface relative to the principal structure axis (Fig. 1c, left). These combined forces drive the post to bend and twist, and thereby expose different faces to the light. Due to this mechanical motion, the direction of molecular alignment will reorient relative to the illumination direction, creating an increasingly

complex travelling front (shown by the dotted purple line in Fig. 1c), which will continuously reorient the principal geometric axis **G**(*t*), enabling the microstructure to flow seamlessly among various deformation modes. Although the overall photoinduced transition is fully reversible, the specific iterative pathway of bimorph evolution is not, enabling inherently non-reciprocal stroke-like motions.

To test the hypothesis and design a representative system, we start with the simple geometry of a high-aspect-ratio square micropost (height = 150 µm; side lengths = 30 µm) (Supplementary Fig. 1). Molecular anisotropy within the micropost was achieved by using liquid crystalline elastomers (LCEs)^{32,33} with the director pre-aligned in an arbitrary orientation using a magnetic field^{34,35} (Fig. 1d, Supplementary Figs. 2–4, Supplementary Methods). Such molecular programmability is distinct from the majority of fabrication methods, which involve either mechanical processing (such as shearing, stretching and 3D printing) in which the LCE director is always parallel to the principal

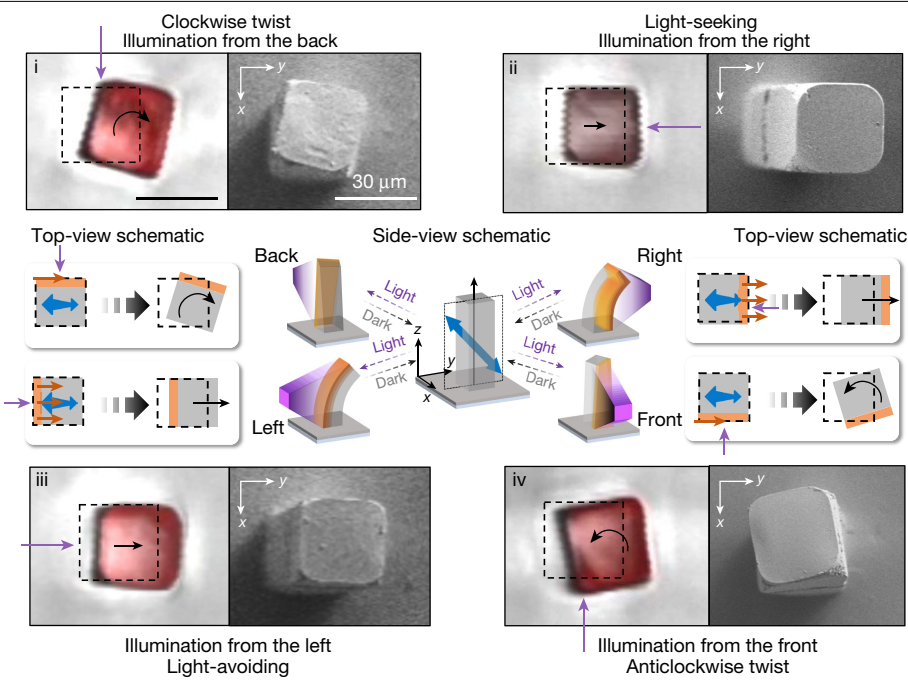


Fig. 2 | In a micropost with oblique director alignment, distinct elementary deformation modes are evoked by irradiation from different directions.

Confocal laser scanning and scanning electron microscopy images of actuated photoreactive LCE microposts with oblique director alignment of $\theta \approx 55^\circ$ (tilted with respect to the principal axis into the yz plane) upon UV irradiation (15 mW cm^{-2}) of four facets (i, ‘back’; ii, ‘right’; iii, ‘left’; and iv, ‘front’). The top-view schematics explain the observed deformation behaviour resulting

from the molecular orientation-induced shearing of the active (orange) layer, which exerts clockwise torque, pull and push, and anticlockwise torque, on the inactive layer, leading to clockwise twisting, bending towards light, bending away from light and anticlockwise twisting of the same microstructure for i–iv, respectively. Director orientation is depicted as a blue double arrow; shear forces are depicted as orange arrows and the resulting movements as black arrows, respectively. Purple arrows indicate illumination direction.

symmetry axis of the microstructure^{19,36–38}, or surface alignment with complex director orientations, but which are only applicable to thin films^{28,29,39}. (Note that magnetic field is only used during the fabrication and not in the subsequent actuation process.) An azobenzene cross-linker was chosen to elicit photomechanical actuation (Fig. 1d, Supplementary Fig. 5), which provides high spatial resolution at the microscale as opposed to the more commonly employed photothermal mechanism (Supplementary Figs. 6, 7)^{40,41}. On exposure to ultraviolet (UV) radiation, azobenzene cross-linkers undergo reversible *trans*-to-*cis* photoisomerization, which mechanically disrupts the local molecular order^{4,41} to create a temporary bimorph inside the post, consisting of an ‘activated’ disordered layer and a ‘non-activated’ nematic phase, as discussed above. We chose a relatively high⁴⁰ concentration of azobenzene cross-linker (7.5 wt%), which restricts light penetration ($\lambda_{\max} = 365 \text{ nm}$) initially to a depth l_B of a few micrometres at mild UV intensity (approximately 15 mW cm^{-2}) according to the Beer–Lambert law $I/I_0 \propto e^{-\epsilon l}$ (l_B defined as l at $1/e$ of I_0 with incident light intensity I_0 , molar attenuation coefficient ϵ and concentration c of the light-absorbing species). Changing the light intensity influences the penetration depth l_B within the post, and the rate with which a photostationary state between the *trans*- and *cis*-isomer is established. Notably, when the light intensity is sufficiently large, a high photostationary state rapidly forms within the first few micrometres, increasing the UV transparency and deepening UV penetration to enable further order-to-disorder conversion of deeper layers, thus creating a travelling isomerization wave^{30,31}. In thin films, such a propagating isomerization front is well known to result in one deformation type—bending towards the light followed by a reversal of direction to an equilibrium position^{30,31} (Supplementary Fig. 8, Supplementary Video 1)—whereas, as we will show below, diverse deformations with non-reciprocal trajectories appear in the system with programmed non-collinear principal axes.

To quantitatively predict the complex opto-chemo-mechanical dynamics and corresponding deformation trajectories of microstructures as a function of the molecular orientation in the constituent LCE material (**M**), the microstructure geometry (**G**) and the direction of illumination (**L**), as well as the light intensity (Fig. 1a), we developed a computational model based on a finite element approach (Supplementary Model 1). The model integrates all the dynamic processes regulating the system (Fig. 1e): the light penetrating into the material, the resultant intensity-dependent photoisomerization and the consequent localized change in the nematic order parameter. The model further couples the order parameter to the strain of the material and reveals the time-dependent evolution of the light-generated bimorph. In this way, it allows us to study and predict in detail how these dynamic processes interact to create the compounding complexity of the deformation pathways. Informed by our finite element model, we demonstrate how these feedback mechanisms make the system amenable to high-resolution programming of diverse motion trajectories, by varying initial conditions, including illumination direction, director orientation, light intensity, microstructure geometry and temperature, and/or by modulation of illumination intervals and duration, as well as extending it to cooperative movements in microstructure arrays and more complex microstructure geometries.

Illumination direction

The unique combination of three non-collinear directional elements (**MGL**) present in our system breaks symmetry differently for each angle of illumination and evokes distinct elementary deformation modes. We experimentally demonstrate four such modes for a chemically uniform microstructure with oblique director illuminated from four sides⁴². As defined by the director, the illuminated ‘activated’ (orange) slab always undergoes a shear, which, depending on the facet of the micropost being illuminated, exerts push/pull forces or clockwise/anticlockwise

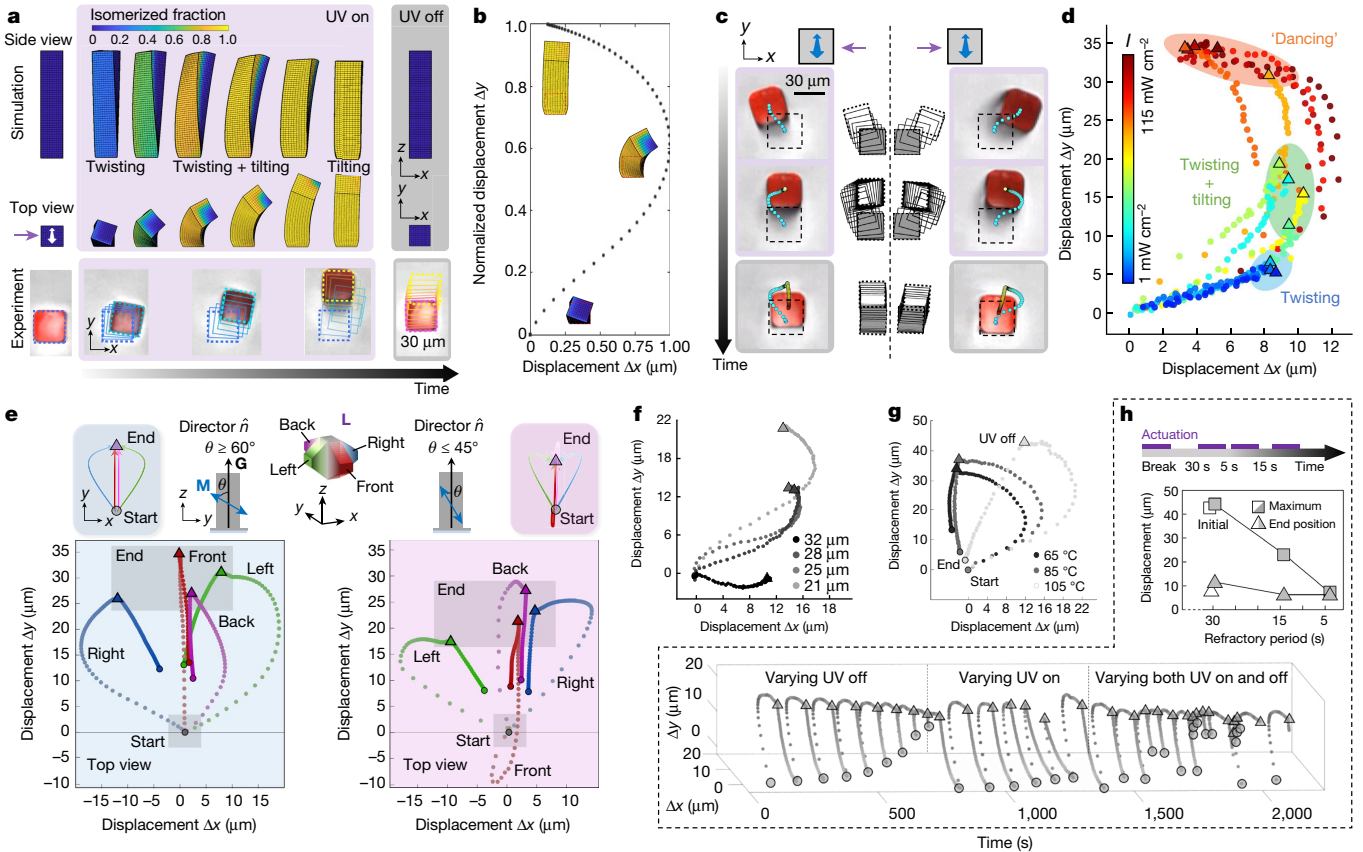


Fig. 3 | High-resolution programming of diverse stroke-like motions. **a**, Juxtaposed computationally simulated (top two rows) and experimental (bottom) data capturing the travelling isomerization wave^{30,31} and complex evolving bimorph resulting from the *trans*- (blue) to *cis*- (yellow) photoisomerization of the azobenzene cross-linker, leading to a stroke-like deformation of the microstructure with oblique director alignment ($\theta = 52^\circ$) at high-intensity illumination (115 mW cm^{-2}). Simulation results were rescaled in time for the experiment. Image tracking overlaid on experimental data (confocal laser scanning microscopy still images, Supplementary Fig. 12) illustrates the deformation trajectory. In image tracking, photoactuation is depicted by the blue-to-yellow transition and thermal relaxation by the yellow-to-red transition. **b**, Predicted normalized deformation trajectory for case in **a** accompanied by top-view rendered simulation still images. **c**, For out-of-plane irradiation (115 mW cm^{-2}) from opposite sides, the same microstructure displays mirrored right- and left-handed curved stroke-like trajectories. **d**, Experimental quantification of different deformation trajectories for 12 light intensities in the range 1– 115 mW cm^{-2} . Circles correspond to the trajectories of the micropost's centre of the top surface during deformation; triangles denote a stable deformed position reached at

the photostationary state. **e**, The director tilt (θ) modulates the relative contribution of the shearing component (along the y axis) and contraction/expansion (along the x axis). Experimental deformation trajectories and their schematic representation for two cases ($\theta = 60^\circ$) and ($\theta = 45^\circ$) for UV irradiations from the front (red), left (green), back (magenta) and right (blue) are shown. Note ‘dancing’ towards or away from the light source, respectively, as is observed by the switch between the green and blue trajectories for the two cases. **f**, **g**, Effect of microstructure thickness (**f**) and temperature (**g**) on deformation trajectories. **h**, The non-instantaneous *cis*-to-*trans* thermal relaxation of the azobenzene cross-linker causes a refractory period between two illumination periods. Top panel illustrates the reduced deformation amplitude with decreasing length of time breaks. Squares correspond to maximum displacement; triangles denote displacement before switching UV off. Bottom panel shows 3D traces of deformation paths along both x and y directions as a function of time under varied illumination duration and intervals, demonstrating deliberately tailored beginning and end points of each actuation path. Circles correspond to starting point of each illumination; triangles denote displacement before switching the UV irradiation off.

torques on the ‘non-activated’ (grey) layer, giving rise to light-seeking, light-avoiding and clockwise or anticlockwise twisting, respectively (Fig. 2, Supplementary Figs. 9–11, Supplementary Video 1). By contrast, heating the structure shows only defined tilting (Supplementary Fig. 10b), as expected for a micropost with an oblique director undergoing a bulk nematic-to-isotropic phase transition. Once the light is switched off, the post directly returns to its original state, because the *cis*-isomer⁴³ is thermally unstable (thermal half-life was determined to be $t_{1/2} = 40 \text{ s}$ in the LCE film at 60°C) (Supplementary Fig. 5).

Illumination intensity

Our finite element model (Supplementary Model 1) shows how, at higher light intensity, multiple types of such motional elements transition seamlessly from one to another through opto-chemo-mechanical

feedback, with complex evolution of the bimorph influencing each subsequent step, as exemplified here in a predicted stroke-like trajectory of a single micropost (Fig. 3a, b): (i) the structure initially twists as a thin illumination layer emerges, which immediately exposes the adjacent new facet to the light; (ii) as the light penetrates further from both facets into the structure, the ‘push’ force and clockwise twist synergistically move the micropost diagonally away from its initial structural axis; and (iii) as the illuminated region grows and starts to take up a majority of the bimorph, backwards bending begins towards a simply tilted micropost, as defined by its nematic director; (iv) when the light is switched off, the structure undergoes a uniform disorder-to-order transition, tilting directly back upright to its initial position, completing a non-reciprocal deformation pathway. We experimentally achieved such self-regulated highly non-linear ‘dancing’ actuation under high

Article

irradiation intensity of 115 mW cm^{-2} (Fig. 3a, bottom, Supplementary Figs. 12, 13, Supplementary Video 2).

When the square micropost is illuminated under high intensity (115 mW cm^{-2}) from either one or the other direction along, for example, the x axis, an identical end position (tilting) governed by the oblique director is achieved when light penetrates through the entire structure (reminiscent of the bulk thermal nematic-to-isotropic phase transition), but mirrored, right- and left-handed, stroke-like actuation paths towards this final state are observed (Fig. 3c, Supplementary Video 3). Movement of the pillar along these trajectories can be further controlled by changing light intensity, which determines where the evolving order-disorder bimorph stabilizes, and, hence, the net force exerted on the post. Figure 3d quantifies these effects at 12 light intensities ($1\text{--}115 \text{ mW cm}^{-2}$) (Supplementary Figs. 13, 14), showing that the same micropost can undergo the twisting motion at lower intensities (as in Fig. 2), but smoothly transitions from twisting to tilting at medium light intensity, and then evolves into an asymmetric, stroke-like movement ('dancing') involving both twisting and tilting outward and inward at maximum light intensity, a behaviour accurately predicted and captured by our simulations (Supplementary Video 2).

Director tilt

We have developed a model that describes how the angle of molecular alignment with respect to the post's geometrical axis (θ) affects the microstructure deformation along the vertical and horizontal directions (Supplementary Model 2, Supplementary Figs. 15, 16). Although the horizontal component is important for shearing within the bimorph, exerting torques and causing twisting motions, the vertical component independently contributes to out-of-plane bending within the trajectory and can be chosen to be either toward ($\theta \geq 60^\circ$) or away from the light ($\theta \leq 45^\circ$) (Fig. 3e). This will lead to 'dancing' toward or away from the light source, respectively. Furthermore, for steep director alignments ($\theta \leq 45^\circ$), a characteristic reversal of motion along the yz plane is observed (Supplementary Figs. 17–19).

Microstructure size

The thickness of the micropost influences not only its effective mechanical stiffness and thus the deformation amplitude, but also the relative size of the 'activated' layer in the evolving bimorph and thus the deformation trajectory (Fig. 3f, Supplementary Fig. 20, Supplementary Video 4). For thicker posts, the out-of-plane movement dominates over the shearing movement and the propagating order-to-disorder transition fades out quickly, leading to a distinctly different deformation trajectory and end point.

Temperature

Simply changing the temperature at which the structure is illuminated provides further methods for high-resolution programming of the motion trajectory. An increase in temperature reduces the material stiffness, which usually enhances deformation amplitude. At the same time, a higher temperature also speeds up the azobenzene *cis*-to-*trans* thermal relaxation, lowering the photostationary state reached and increasing the fraction of the *trans*-azobenzene corresponding to reduced UV transparency. Hence, the progression of the travelling isomerization front stops earlier. These two effects work synergistically to influence the actuation trajectory (Fig. 3g, Supplementary Fig. 21, Supplementary Video 4) to a larger out-of-plane motion. Note that ample means are available for speeding up the deformation by decreasing the thickness of the micropost, lowering the concentration of the azobenzene cross-linkers or extending to other photochemistries³³.

Irradiation duration and intervals

As discussed, the activated photoswitchable cross-linker thermally returns to its *trans*-isomer within the LCE, and the microstructure relaxes to its original upright state within seconds to minutes after

the light is switched off. If irradiation is renewed during this 'refractory period' when a majority of azobenzene cross-linkers is still in the *cis*-form, only marginal deformation occurs. Leveraging this effect, the starting and end position, as well as the amplitude of the arc and path of relaxation of the deforming pillar, can be precisely chosen by controlling the illumination duration and intervals, producing a rich 'dancing' behaviour with no noticeable fatigue for over 100 cycles (Fig. 3h, Supplementary Figs. 22–24, Supplementary Video 5).

Cooperative movements in arrays of microstructures

As one expands the system from a single micropost to strings of microstructures or two-dimensional (2D) arrays (produced by a simple moulding procedure), additional symmetry axes (degrees of freedom) are added to the system, which in the simplest case of a one-dimensional (1D) array can be captured by the array axis \mathbf{G}_a defined in terms of a string direction and interpillar distance, w . We explored the potential for dynamic pattern evolution and emergent communication between the microstructures in such a system using a string of circular microposts with z -aligned mesogens (\mathbf{G} and \mathbf{M} collinear) (Fig. 4a–d). If \mathbf{G}_a and \mathbf{L} are perfectly aligned, one would expect only bending towards the light (along the string axis) with rapidly decreasing amplitude. However, as schematically presented in Supplementary Fig. 25, with even a small misalignment between \mathbf{G}_a and \mathbf{L} (shown as angle δ), the first pillar would bend slightly out of line, leading to asymmetric exposure of the next pillar and creating a bimorph that bends out of the string axis in an opposite direction, with bending amplitude and symmetry breaking amplified along the string in a distance- and location-dependent manner. To capture such a unique collective response in pillar arrays, we developed a simplified discrete model that considers how the interpillar communication changes what parts of neighbouring microstructures become illuminated on directional light exposure (Supplementary Model 3, Supplementary Fig. 26). Our simulations, confirmed by the follow-up experiments, show that in pairs of z -aligned microposts of different interpost spacing w ($w = 45, 65$ or $130 \mu\text{m}$), for a small δ , symmetry breaking arises at $w = 65 \mu\text{m}$, whereas at short distances no actuation of the mostly shadowed second post occurs and at long distances 'decoupled', identical bending towards the light of both posts is observed (Fig. 4a). In longer strings, such distance-dependent symmetry breaking leads to a stable and repeatedly reproducible wave-like pattern (Fig. 4b), a behaviour accurately captured by both our finite element simulations (Supplementary Fig. 27) and a simplified mathematical model (Fig. 4b, right). The spontaneous asymmetry amplification endows the system with a high sensitivity to any $\mathbf{G}_a\mathbf{LM}$ non-collinearity and access to drastically different self-sorted patterns (Supplementary Figs. 28, 29, Supplementary Video 6). The degree of interpillar coupling and thus self-organization depends strongly on the magnitude of misalignment, δ , most effectively demonstrated in a 2D square array of microposts containing \mathbf{G}_a (axis along the nearest neighbour) and \mathbf{G}_{ad} (direction along the diagonal) axes. As the array is illuminated along the \mathbf{G}_a or \mathbf{G}_{ad} direction, the effective interpost spacing changes, thus enhancing or suppressing the interpost communication (Fig. 4c, Supplementary Video 7).

We further note that under conditions that allow for dynamic bimorph propagation locally within each single pillar (as described in Fig. 3), a unique, 'global' deformation front is expected to travel concurrently at the ensemble level (with a different propagation velocity) dependent on the effective pillar density along the light path. Indeed, we showcase in a radially arranged microarray with z -aligned mesogens (Fig. 4d) that when the array is illuminated, these interacting propagation fronts lead to a complex evolution of the travelling wave of the communicating posts at the ensemble level. In this radial arrangement, the multiple \mathbf{G}_a axes have different relative orientations to \mathbf{L} , resulting in various local hierarchical spacings along the light path and causing the complexity of the collective travelling front (Supplementary Video 7). Moreover, if \mathbf{G} and \mathbf{M} are non-collinear within each micropost, one would expect that in a 2D array, the previously described

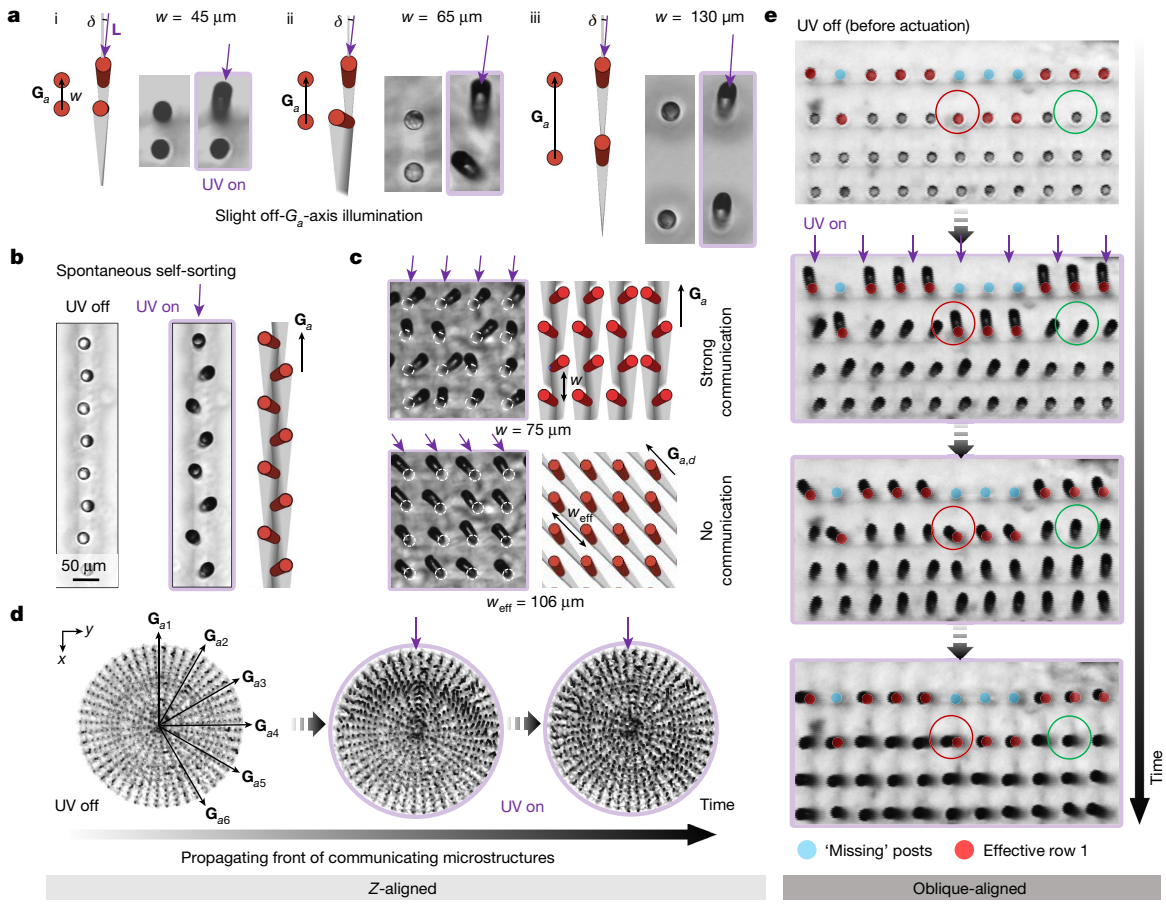


Fig. 4 | Collective self-regulated deformation dynamics in arrays of microposts. **a**, Simulation (left) and experimental (right) results of the light response of pairs of microposts, when the illumination direction, \mathbf{L} , forms a small angle, δ , with the pair axis, \mathbf{G}_a , illustrating how different interpost spacings, w , influence the deformation trajectory of subsequent posts. **b**, Spontaneous self-organization of appropriately spaced strings of microposts into an undulating line. Modelling results are shown on the right. **c**, For a square 2D microarray, strong interpost communication and coupled undulating deformations occur when light comes along the nearest neighbour

direction (\mathbf{G}_a , $w = 75 \mu\text{m}$), and decoupled uniform light-seeking motions when illuminated along the diagonal ($\mathbf{G}_{a,d}$, $w = 106 \mu\text{m}$). Left: experiment; right: simulation. **d**, Formation of a complex travelling wave of locally interacting posts in a radially arranged microarray, demonstrating a rich ensemble dynamics. **e**, Amplification of engineered ‘defects’ in arrays of oblique-aligned microposts: missing microstructures alter the local illumination conditions and interpillar spacing and change the deformation trajectories of the posts around them, and thus the overall ensemble dynamics. Optical microscopic images of the illuminated posts in **a–e** are outlined in purple.

‘dancing’ motions of each post would adapt to and self-organize with the motion of their neighbours, with each post undergoing a unique position-dependent trajectory (Supplementary Fig. 30). Together with programmed defects (for example, missing pillars), one can therefore construct micropost ensembles with highly controlled, emergent time- and location-dependent deformation trajectories (Fig. 4e). For example, two microposts (circled in red and green) from the same row in the array exhibit completely different deformation trajectories yet start and end at similar states (Fig. 4e, Supplementary Video 8).

More complex geometries

In free-standing, jointed, compositionally uniform microstructures, the presence of multiple geometrical axes (in this case $\mathbf{G}_{\text{segment}}$, the principal symmetry axis of each constitutive part) provides additional opportunities for cooperative complex deformation patterns, such as stirring, bowing or bird-like motions, arising from distinct relative $\mathbf{G}_{\text{segment}}$ - \mathbf{ML} orientations and thus distinct local symmetry breakings and corresponding motions for each constitutive part. For example, an X-shaped actuator exhibits programmable deformations that include mutually opposite right- and left-handed twisting and bending of the $\mathbf{G}_{\text{segment}}^{13}$ and $\mathbf{G}_{\text{segment}}^{24}$ reminiscent of crawlers or the wing-warping/twisting necessary for bird flight (Fig. 5a, Supplementary Figs. 31–33, Supplementary Video 9). The helicity and extent of

twisting and closure/opening or out-of-plane movements of the arms can be judiciously chosen through variations of relative orientations of \mathbf{L} , \mathbf{M} and geometric axes of each arm. By contrast, thermal heating of the X-shaped actuator shows only one deformation—a direct shrinkage along the molecular alignment to a ‘slender’ X without undergoing any twisting (Supplementary Fig. 34). Furthermore, if one end of the arm ($\mathbf{G}_{\text{segment}}^{13}$) now serves as an anchoring point, a greatly amplified twist of $\mathbf{G}_{\text{segment}}^{24}$ fully coupled to the motion of $\mathbf{G}_{\text{segment}}^{13}$ is observed. This implies that such actuators can serve as micro-joints/hinges with the ability to control a variety of motion trajectories of macroscale pieces. Our computational method enables us to further explore a library of combinations of $\mathbf{G}_{\text{segment}}$ - \mathbf{ML} and show deformations, including ‘stirring’, and catching or releasing cargo (Supplementary Video 10). As an illustration, Fig. 5b models diverse motions of T-, L- and palm-tree-shaped compositionally uniform actuators undergoing multiple, evolving in time, deformations depending on the light direction. Non-symmetrical movements of different arms can be readily achieved by shifting the illumination direction away from the structure-symmetric axes or having off-axis director orientation (Supplementary Fig. 35). The ramifications for microscopic soft robots capable of a tremendous set of motions are immediate and numerous.

To conclude, we present a strategy for programming various self-regulated, stroke-like dancing trajectories in a single,

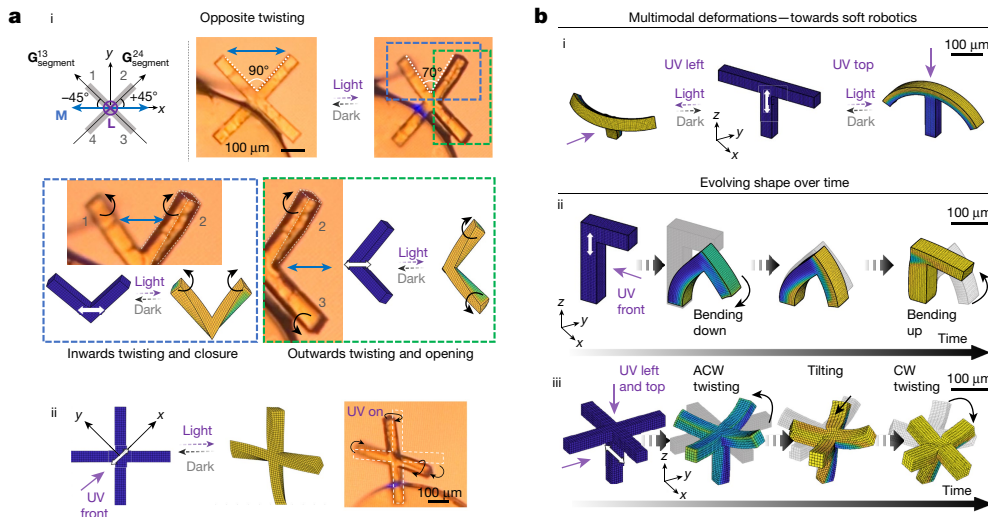


Fig. 5 | Higher order self-regulated dynamics in jointed compositionally uniform microactuators. **a, i**, In a free-standing X-shaped actuator containing two perpendicular structural axes G_{segment}^{13} and G_{segment}^{24} , which form $+45^\circ$ and -45° with the uniform director orientation, **M** (shown as a blue double arrow), bending and twisting motions of opposite direction can be invoked for different arms within the same single-material, moulded microstructure. Magnified photographs and corresponding theoretical simulations depicting the motion of the top two and the right two segments of the structure are shown below in blue and green insets, respectively. **ii**, With one arm being the anchoring spot, the twisting of G_{segment}^{24} couples to the twisting/rotation of the

G_{segment}^{13} axis, demonstrating amplification of the sway motion through the arms in both simulations and experiments. **b**, Simulation results for diverse motions in: (i) T-shape with global vertical molecular alignment that undergoes distinct deformations for different light directions (i); L-shape actuator with global vertical molecular alignment, illustrating a programmable movement sequence of bending down and upwards in a single UV actuation period, as a travelling light front propagates through the structure (ii); palm-tree-shaped actuator with oblique molecular alignment, illustrating a progressive anticlockwise (ACW) and clockwise (CW) twisting accompanied by the closure and opening of the arms (iii).

compositionally uniform microstructure fabricated by a simple moulding procedure. The self-regulatory behaviour is fundamentally different from existing feedback systems: due to the imposed non-collinearity of **MLG** axes, light propagating through the material generates a transient, dynamically evolving bimorph with increasingly complex symmetry breaking along the front, specifying a diversity of motion pathways composed of different deformation types—composites of twisting, bending, light seeking and light avoiding. The resulting range of actuations cannot be achieved with existing approaches that involve complicated multilayered architectures, 3D printing or direct manipulation, especially for 3D structures in the 10–100 μm size range. Our simulations quantitatively capture this multilevel opto-chemo-mechanical feedback dynamics, enabling us to theoretically predict and experimentally programme the spatiotemporal behaviour of nearly infinite actuation pathways. The core design principles presented here can be applied to other anisotropic materials, such as fibre-reinforced hydrogels^{44,45} or shape-shifting crystals⁴⁶, and extended to include different photochemistries³³, and polarized or dynamic light sources.

Furthermore, this self-regulated bimorph dynamics has marked implications for eliciting complex collective behaviours in microstructure arrays, in which **MLG** reorientations involving additional geometrical axes ($\mathbf{G}_{\text{array}}$) lead to distinct position-dependent symmetry breaking and unique motion pathways for each micropost. The interpillar communication and multilevel propagation dynamics we demonstrate reveal the fundamental scalability and predictability of the designed feedback mechanism beyond a single microstructure, and provide the means to control the collective behaviour in microstructure ensembles. The observed emergent behaviours, such as bistability, stable wave-like patterns and sensitivity to small perturbations, are typically hallmarks of complexity⁴⁷ in multicomponent systems that rely on molecular-scale, diffusion or flow-limited processes, such as chemical reaction networks^{48–50} or even chemo-mechanical actuators^{27,28}, but here complexity emerges from the simplicity of the single-material photoresponsive system. The design concepts introduced herein also lead to bird-like

and other complex programmed motions in free-standing jointed single-material microstructures with multiple non-aligned $\mathbf{G}_{\text{segment}}$ axes. This vast design space for individual and collective motions is potentially transformative for fields ranging from soft robotics, micro-walkers, sensors and cell culture scaffolds to robust information encryption systems in which information encoded in an array can be read out by an infinite number of different dynamic patterns evoked by different illumination directions, intensities, durations, intervals, as well as wavelengths and polarizations.

Online content

Any methods, additional references, Nature Research reporting summaries, source data, extended data, supplementary information, acknowledgements, peer review information; details of author contributions and competing interests; and statements of data and code availability are available at <https://doi.org/10.1038/s41586-022-04561-z>.

1. Sleigh, M. A. *The Biology of Cilia and Flagella* (Pergamon Press, 1962).
2. Gilpin, W., Bull, M. S. & Prakash, M. The multiscale physics of cilia and flagella. *Nat. Rev. Phys.* **2**, 74–88 (2020).
3. Hu, W., Lum, G. Z., Mastrangeli, M. & Sitti, M. Small-scale soft-bodied robot with multimodal locomotion. *Nature* **554**, 81–85 (2018).
4. Van Oosten, C. L., Bastiaansen, C. W. M. & Broer, D. J. Printed artificial cilia from liquid-crystal network actuators modularly driven by light. *Nat. Mater.* **8**, 677–682 (2009).
5. Gu, H. et al. Magnetic cilia carpets with programmable metachronal waves. *Nat. Commun.* **11**, 2637 (2020).
6. Rus, D. & Tolley, M. T. Design, fabrication and control of soft robots. *Nature* **521**, 467–475 (2015).
7. Huang, H. W., Sakar, M. S., Petruska, A. J., Pané, S. & Nelson, B. J. Soft micromachines with programmable motility and morphology. *Nat. Commun.* **7**, 12263 (2016).
8. Wu, Z. L. et al. Three-dimensional shape transformations of hydrogel sheets induced by small-scale modulation of internal stresses. *Nat. Commun.* **4**, 1586 (2013).
9. Tottori, S. et al. Magnetic helical micromachines: fabrication, controlled swimming, and cargo transport. *Adv. Mater.* **24**, 811–816 (2012).
10. Wehner, M. et al. An integrated design and fabrication strategy for entirely soft, autonomous robots. *Nature* **536**, 451–455 (2016).
11. Yan, X. et al. Multifunctional biohybrid magnetite microrobots for imaging-guided therapy. *Sci. Robot.* **2**, eaq1155 (2017).

12. Nelson, B. J., Kaliakatsos, I. K. & Abbott, J. J. Microrobots for minimally invasive medicine. *Annu. Rev. Biomed. Eng.* **12**, 55–85 (2010).
13. Osada, Y. & Rossi, D. D. *Polymer Sensors and Actuators* (Springer, 2013).
14. Noorduin, W. L., Grinthal, A., Mahadevan, L. & Aizenberg, J. Rationally designed complex, hierarchical microarchitectures. *Science* **340**, 832–837 (2013).
15. Lerch, M. M., Grinthal, A. & Aizenberg, J. Viewpoint: homeostasis as inspiration—toward interactive materials. *Adv. Mater.* **32**, 1905554 (2020).
16. Hippel, M. et al. Controlling the shape of 3D microstructures by temperature and light. *Nat. Commun.* **10**, 232 (2019).
17. Lahikainen, M., Zeng, H. & Priimagi, A. Design principles for non-reciprocal photomechanical actuation. *Soft Matter* **16**, 5951–5958 (2020).
18. Kim, Y., Yuk, H., Zhao, R., Chester, S. A. & Zhao, X. Printing ferromagnetic domains for untextured fast-transforming soft materials. *Nature* **558**, 274–279 (2018).
19. Kotikian, A., Truby, R. L., Boley, J. W., White, T. J. & Lewis, J. A. 3D printing of liquid crystal elastomeric actuators with spatially programmed nematic order. *Adv. Mater.* **30**, 1706164 (2018).
20. Lahikainen, M., Zeng, H. & Priimagi, A. Reconfigurable photoactuator through synergistic use of photochemical and photothermal effects. *Nat. Commun.* **9**, 4148 (2018).
21. Palagi, S. et al. Structured light enables biomimetic swimming and versatile locomotion of photoresponsive soft microrobots. *Nat. Mater.* **15**, 647–653 (2016).
22. Yan, Z. et al. Mechanical assembly of complex, 3D mesostructures from releasable multilayers of advanced materials. *Sci. Adv.* **2**, e1601014 (2016).
23. Zhang, H., Koens, L., Lauga, E., Mourran, A. & Möller, M. A light-driven microgel rotor. *Smal* **15**, 1903379 (2019).
24. Zhang, Y. et al. Seamless multimaterial 3D liquid-crystalline elastomer actuators for next-generation entirely soft robots. *Sci. Adv.* **6**, eaay8606 (2020).
25. Qian, X. et al. Artificial phototropism for omnidirectional tracking and harvesting of light. *Nat. Nanotechnol.* **14**, 1048–1055 (2019).
26. Aizenberg, M., Okeyoshi, K. & Aizenberg, J. Inverting the swelling trends in modular self-oscillating gels crosslinked by redox-active metal bipyridine complexes. *Adv. Funct. Mater.* **28**, 1704205 (2018).
27. He, X. et al. Synthetic homeostatic materials with chemo-mechano-chemical self-regulation. *Nature* **487**, 214–218 (2012).
28. Gelebart, A. H. et al. Making waves in a photoactive polymer film. *Nature* **546**, 632–636 (2017).
29. Serak, S. et al. Liquid crystalline polymer cantilever oscillators fueled by light. *Soft Matter* **6**, 779–783 (2010).
30. Corbett, D. & Warner, M. Linear and nonlinear photoinduced deformations of cantilevers. *Phys. Rev. Lett.* **99**, 174302 (2007).
31. Corbett, D., Van Oosten, C. L. & Warner, M. Nonlinear dynamics of optical absorption of intense beams. *Phys. Rev. A* **78**, 013823 (2008).
32. White, T. J. & Broer, D. J. Programmable and adaptive mechanics with liquid crystal polymer networks and elastomers. *Nat. Mater.* **14**, 1087–1098 (2015).
33. Bisoyi, H. K. & Li, Q. Light-driven liquid crystalline materials: from photo-induced phase transitions and property modulations to applications. *Chem. Rev.* **116**, 15089–15166 (2016).
34. Buguin, A., Li, M. H., Silberzan, P., Ladoux, B. & Keller, P. Micro-actuators: when artificial muscles made of nematic liquid crystal elastomers meet soft lithography. *J. Am. Chem. Soc.* **128**, 1088–1089 (2006).
35. Yao, Y. et al. Multiresponsive polymeric microstructures with encoded predetermined and self-regulated deformability. *Proc. Natl. Acad. Sci. USA* **115**, 12950–12955 (2018).
36. Küpper, J. & Finkelmann, H. Nematic liquid single crystal elastomers. *Makromol. Chem. Rapid Commun.* **12**, 717–726 (1991).
37. Liu, L. et al. Light tracking and light guiding fiber arrays by adjusting the location of photoresponsive azobenzene in liquid crystal networks. *Adv. Opt. Mater.* **8**, 2000732 (2020).
38. Lin, X., Saed, M. O. & Terentjev, E. M. Continuous spinning aligned liquid crystal elastomer fibers with a 3D printer setup. *Soft Matter* **17**, 5436–5443 (2021).
39. Ware, T. H., McConney, M. E., Wie, J. J., Tondiglia, V. P. & White, T. J. Voxelated liquid crystal elastomers. *Science* **347**, 982–984 (2015).
40. Pilz Da Cunha, M., Van Thoor, E. A. J., Debije, M. G., Broer, D. J. & Schenning, A. P. H. J. Unravelling the photothermal and photomechanical contributions to actuation of azobenzene-doped liquid crystal polymers in air and water. *J. Mater. Chem. C* **7**, 13502–13509 (2019).
41. Barrett, C. J., Mamiya, J. I., Yager, K. G. & Ikeda, T. Photo-mechanical effects in azobenzene-containing soft materials. *Soft Matter* **3**, 1249–1261 (2007).
42. Waters, J. T. et al. Twist again: dynamically and reversibly controllable chirality in liquid crystalline elastomer microposts. *Sci. Adv.* **6**, eaay5349 (2020).
43. Serra, F. & Terentjev, E. M. Effects of solvent viscosity and polarity on the isomerization of azobenzene. *Macromolecules* **41**, 981–986 (2008).
44. Erb, R. M., Sander, J. S., Grisch, R. & Studart, A. R. Self-shaping composites with programmable bioinspired microstructures. *Nat. Commun.* **4**, 1712 (2013).
45. Sydney Gladman, A., Matsumoto, E. A., Nuzzo, R. G., Mahadevan, L. & Lewis, J. A. Biomimetic 4D printing. *Nat. Mater.* **15**, 413–418 (2016).
46. Karothu, D. P. et al. The rise of the dynamic crystals. *J. Am. Chem. Soc.* **31**, 13256–13272 (2020).
47. Kaspar, C., Ravoo, B. J., van der Wiel, W. G., Wegner, S. V. & Pernice, W. H. P. The rise of intelligent matter. *Nature* **594**, 345–355 (2021).
48. Turiv, T. et al. Topology control of human fibroblast cells monolayer by liquid crystal elastomer. *Sci. Adv.* **6**, p.eaaz6485 (2020).
49. Hauser, A. W., Sundaram, S. & Hayward, R. C. Photothermocapillary oscillators. *Phys. Rev. Lett.* **121**, 158001 (2018).
50. Babu, D. et al. Acceleration of lipid reproduction by emergence of microscopic motion. *Nat. Commun.* **12**, 2959 (2021).

Publisher's note Springer Nature remains neutral with regard to jurisdictional claims in published maps and institutional affiliations.

© The Author(s), under exclusive licence to Springer Nature Limited 2022

Article

Methods

Fabrication of LCE microstructures

The mixtures of liquid crystalline monomers, photoinitiator and azobenzene cross-linker were first made molten into the negative mould of the desired microstructures, covered with a coverslip and then slowly cooled to 60 °C. The mould with the prepolymer mixture was placed oriented in a weak magnetic field (approximately 0.5 T, NdFeB) to align the mesogens in an arbitrary direction relative to the microstructure principal axis. This molecular anisotropy was locked-in to the resulting LCE microstructures by UV polymerization, after which the sample was cooled down to room temperature and the mould was carefully peeled off.

Imaging of the LCE microstructure actuation

Microstructures were imaged by scanning electron microscopy. The thermal or photoactuation behaviour of LCE microstructures was studied by confocal fluorescence laser scanning microscopy, for which microstructures were stained with a Rhodamine B dye and imaged with 555 nm light focused on the top face of the microposts. For directional photoactuation with a 365 nm UV LED (Thorlabs M365F1), the microstructures were heated to 60 °C (above their glassy state, $T_g \approx 45$ °C) and deformation trajectories were followed as time series and by adjusting the focal plane as the posts deformed. The time series were subsequently image tracked using a MATLAB script. The scanning electron microscopy images of the deformed LCE microposts were obtained by ‘trapping’ the actuated shape in the glassy state of the LCE by rapidly cooling from 60 °C to room temperature.

Finite element simulations

Simulations were carried out using a custom finite element code written in C++, accounting for the energy of shear and bulk deformations of the elastomer, as well as a strain–nematic coupling proportional to the change in the order parameter, assumed to be proportional to the fraction of *cis*-isomers. At each time step, the isomerization at each mesh node was updated on the basis of the light intensity, computed by ray tracing through the finite element mesh and applying an attenuation derived from the isomerized fraction at that point in time.

Discrete model for arrays of microstructures

A simple discrete model was established to investigate the collective responses of arrays of microposts on directional irradiation. At each

time step, shadows created by the microposts were calculated and updated on the basis of the locations of the posts. The neighbouring shadows determine the illumination condition of each post, which in turn govern their deformation. The micropost array can therefore be modelled as a set of dynamic equations, which were solved by the Runge–Kutta method using MATLAB.

Data availability

The data supporting the findings of this study are included within the paper and its Supplementary Information files and are available from the corresponding author upon request.

Code availability

All codes needed to evaluate the conclusions in the paper are present in the paper and/or the Supplementary Information. Additional data related to this paper are available from the corresponding author upon request.

Acknowledgements This work was primarily supported by the US Army Research Office, under grant number W911NF-17-1-0351. K.B. and B.D. were supported by the National Science Foundation (NSF) through the Harvard University Materials Research Science and Engineering Center (MRSEC) under award DMR-2011754. M.M.L. was supported by the Netherlands Organization for Scientific Research (NWO, Rubicon Fellowship 019.182EN.027). Microfabrication and scanning electron microscopy were performed at the Center for Nanoscale Systems (CNS) at Harvard, a member of the National Nanotechnology Coordinated Infrastructure Network (NNCI), supported by the NSF ECCS award no. 1541959. We thank M. Aizenberg, M. Pilz Da Cunha, M. Liu, A. Chen and Y. Zhao for discussions.

Author contributions S.L., M.M.L. and J.A. conceived the project. S.L. and Y.Y. synthesized the side-on LCE monomer used for fabrication. S.L., M.M.L., R.S.M. and D.Y.K. performed the experiments. B.D. and K.B. performed theoretical modelling and image tracking. A.C.B. and J.T.W. performed finite element modelling. S.L., M.M.L., A.G., R.S.M. and B.D. analysed the experimental data. J.A. supervised the project. All co-authors provided useful feedback and contributed to the manuscript.

Competing interests The authors declare no competing interests.

Additional information

Supplementary information The online version contains supplementary material available at <https://doi.org/10.1038/s41586-022-04561-z>.

Correspondence and requests for materials should be addressed to Joanna Aizenberg.

Peer review information *Nature* thanks Peter Hesketh and the other, anonymous, reviewer(s) for their contribution to the peer review of this work.

Reprints and permissions information is available at <http://www.nature.com/reprints>.